Available online at www.elixirpublishers.com (Elixir International Journal)

Computational Chemistry

Elixir Comp. Chem. 70 (2014) 24318-24325

ISSN: 2229-712X

Structures and vibrational frequencies of 2,3,6-trimethylphenol based on density functional theory calculations

M.K.Subramanian* and A.Manaka

Post Graduate and Research Department of Physics, Thiruvalluvar Government Arts College, Rasipuram, India.

ARTICLE INFO

Article history:

Received: 15 February 2014;

Received in revised form:

10 May 2014;

Accepted: 20 May 2014;

Keywords

Density Functional Theory,
FT-Raman,
FT-IR,
HOMO,
LUMO,
First-order Hyperpolarizability,
Electronic Excitation Energy.

ABSTRACT

The FT-IR and FT-Raman spectra of 2,3,6-trimethylphenol (236TMP) were recorded in the regions 4000-400 cm^{-1} and 4000-100 cm^{-1}. The fundamental vibrational frequencies and intensity of vibrational bands were evaluated using density functional theory (DFT) and standard B3LYP/6-311+G** basis set combination. The vibrational spectra were interpreted, with the aid of normal coordinate analysis based on a scaled quantum mechanical (SQM) force field. The Infrared and Raman spectra were also predicted from the calculated intensities. Comparison of simulated spectra with the experimental spectra provides important information about the ability of the computational method to describe the vibrational modes. Unambiguous vibrational assignment of all the fundamentals was made using the total energy distribution (TED). Further, density functional theory (DFT) combined with quantum chemical calculations to determine the first-order hyperpolarizability. The calculated HOMO and LUMO energies shows that charge transfer occur within the molecule. Electronic excitation energies, oscillator strength and nature of the respective excited states were calculated by the closed-shell singlet calculation method were also calculated for the molecule.

Introduction

Phenol (also known as carbolic acid and phenic acid) is used in the treatment of localized skin disorders and as a local anesthetic. Dilute phenol solutions have been injected for celiac plexus nerve blocks. It is also used extensively in the manufacture of many other chemicals and drugs, as a dye and indicator, antiseptic, disinfectant, a reagent in chemical analysis, and a preservative for pharmaceuticals. It is Intermediate for Synthetic Vitamin E Antioxidants and Plastics.

2,3,6-Trimethylphenol's production and use as a comonomer for the modification of polyphenylene oxide resins and as a starting material in vitamin E synthesis may result in its release to the environment through various waste streams. If released to air, a vapor pressure of 0.035 mm Hg at 25 deg C indicates 2,3,6-trimethylphenol will exist solely as a vapor in the ambient atmosphere. Vapor-phase 2,3,6-trimethylphenol will be degraded in the atmosphere by reaction with photochemically-produced hydroxyl radicals; the half-life for this reaction in air is estimated to be 3 hours. If released to soil, 2,3,6-trimethylphenol is expected to have low mobility based upon an estimated Koc of 700. Volatilization from moist soil surfaces is expected to occur slowly based upon an estimated Henry's Law constant of 3.9X10-6 atm-cu m/mole. 2,3,6-Trimethylphenol is not expected to volatilize from dry soil surfaces based on its vapor pressure. If released into water, 2,3,6-trimethylphenol is expected to adsorb to suspended solids and sediment in the water column based upon the estimated Koc. Volatilization from water surfaces is expected based upon this compound's estimated Henry's Law constant. Estimated volatilization half-lives for a model river and model lake are 11 and 84 days, respectively. The potential for bioconcentration in aquatic organisms is moderate based on an estimated BCF value of 60. This compound is not expected to undergo hydrolysis in the environment due to the lack of hydrolyzable functional groups. Occupational exposure to 2,3,6-trimethylphenol may occur through inhalation and dermal contact with this compound at workplaces where 2,3,6-trimethylphenol is produced or used.

In the present study, we report the vibrational analysis of 2,3,6-trimethylphenol (236TMP) using the SQM force field method based on density functional theory (DFT) calculations. The calculated infrared and Raman spectra of the title compounds were simulated utilizing the scaled force fields and the computed dipole derivatives for IR intensities and polarisability derivatives for Raman intensities. The first-order hyperpolarizibility (β_{ijk}) of the novel molecular system is calculated using 3-21 G (d,p) basis set based on finite field approach.

Experimental details

The fine sample of 236TMP were purchased from Lancaster chemical company U.K., and used as such for the spectral measurements. The room temperature Fourier transform infrared spectrum of the title compound was measured with KBr pellet technique in the 4000–400 cm^{-1} region at a resolution of 1 cm^{-1} using BRUKER IFS 66v FTIR spectrometer equipped with a cooled MCT detector for the mid-IR range. Boxcar apodization was used for the 250 averaged interferograms collected for the sample and background. The FT-Raman spectrum was recorded at a BRUCKER IFS-66v model interferometer equipped with an FRA–106 FT-Raman accessory. The spectrum was recorded in the 3500–100 cm^{-1} stokes region using 1064 nm line of a Nd:YAG laser for excitation operating at 200mW power.

Computational details

In order to find the most optimized molecular geometry, the energy and vibrational frequency calculations were carried out for 236TMP with GAUSSIAN 03W software package [1] using the B3LYP functional [2] standard 6-311+G** (large) basis sets. The Cartesian representation of the theoretical force constants

Tele:
E-mail addresses: profdrmks@gmail.com

have been computed at optimized geometry by assuming Cs point group symmetry. Scaling of the force field was performed according to the SQM procedure [3] using selective scaling in the natural internal coordinate representation. Transformation of the force field and subsequent normal coordinate analysis including the least square refinement of the scale factors, calculation of the total energy distribution (TED) and the prediction of IR and Raman intensities were done on a PC with the MOLVIB program (version 7.0-G77) written by Sundius [4]. For the plots of simulated IR and Raman spectra, pure Lorentizian band shapes were used with a bandwidth of 10 cm^{-1}.

The symmetry of the molecule was also helpful in making vibrational assignments. The symmetries of the vibrational modes were determined by using the standard procedure [5] of decomposing the traces of the symmetry operation into the irreducible representations. The symmetry analysis for the vibrational mode of 236TMP is presented in some details in order to describe the basis for the assignments. By combining the results of the GAUSSVIEW program [6] with symmetry considerations, vibrational frequency assignments were made with a high degree of confidence.

The Raman activities (Si) calculated with the GAUSSIAN 03W program and adjusted during the scaling procedure with MOLVIB were subsequently converted to relative Raman intensities (Ii) using the following relationship derived from the basic theory of Raman scattering [7-9].

$$I_i = \frac{f(v_o - v_i)^4 S_i}{v_i[1-\exp(-hcv_i / KT)} \quad \text{----------(1)}$$

Where υ_0 is the exciting frequency (in cm^{-1}), υ_i is the vibrational wavenumber of the i^{th} normal mode; h, c and k are fundamental constants, and f is a suitably chosen common normalization factor for all peak intensities.

Essentials of nonlinear optics related to β

The nonlinear response of an isolated molecule in an electric field $E_i(\omega)$ can be represented as a Taylor expansion of the total dipole moment μ_t induced by the field:

$$\mu_t = \mu_0 + \alpha_{ij}E_i + \beta_{ijk}E_iE_j + ...$$

Where α is linear polarizability, μ_0 the permanent dipole moment and β_{ijk} are the first-order hyperpolarizability tensor components.

The components of first-order hyperpolarizability can be determined using the relation

$$\beta_i = \beta_{iii} + \frac{1}{3}\sum_{i \neq j}(\beta_{ijj} + \beta_{jij} + \beta_{jji})$$

Using the x, y and z components the magnitude of the total static dipole moment (μ), isotropic polarizability (α_0), first-order hyperpolarizability (β_{total}) tensor, can be calculated by the following equations:

$$\mu_1^0 = (\mu_x^2 + \mu_y^2 + \mu_z^2)^{1/2}$$

$$\beta_{tot} = (\beta_x^2 + \beta_y^2 + \beta_z^2)^{1/2}$$

The complete equation for calculating the first-order hyperpolarizability from GAUSSIAN 03W output is given as follows:

$$\beta_{tot} = [(\beta_{xxx} + \beta_{xyy} + \beta_{xzz})^2 + (\beta_{yyy} + \beta_{yzz} + \beta_{yxx})^2 + (\beta_{zzz} + \beta_{zxx} + \beta_{zyy})^2]$$

The β components of GAUSSIAN 03W output are reported in atomic units, the calculated values have to be converted into electrostatic units (1 a.u= 8.3693 $x10^{-33}$ esu).

Before calculating the hyperpolarizability for the in-vestigated compound, the optimization has been carried out in the UHF (unrestricted open-shell Hartree-Fock) level. Molecular geometries were fully optimized by Berny's optimization algorithm using redundant internal coordinates. All optimized structures were confirmed to be minimum energy conformations. An optimization is complete when it has converged. i.e., when it has reached a minimum on the potential energy surface, thereby predicting the equilibrium structures of the molecules. This criterion is very important in geometry optimization. The inclusion of d polarization and double zeta function in the split valence basis set is expected to produce a marked improvement in the calculated geometry. At the optimized structure, no imaginary frequency modes were obtained proving that a true minimum on the potential energy surface was found. The electric dipole moment and dispersion free first-order hyperpolarizibility were calculated using finite field method. The finite field method offers a straight forward approach to the calculation of hyperpolarizabilities. All the calculations were carried out at the DFT level using the three-parameter hybrid density functional B3LYP and a 6-311+G** basis set.

Results and discussion

Molecular geometry

The global minimum energy obtained by the DFT structure optimization was presented in Table 1. The optimized geometrical parameters obtained by the large basis set calculation were presented in Table 2. The optimized molecular structure of 236TMP was shown in Fig. 1.

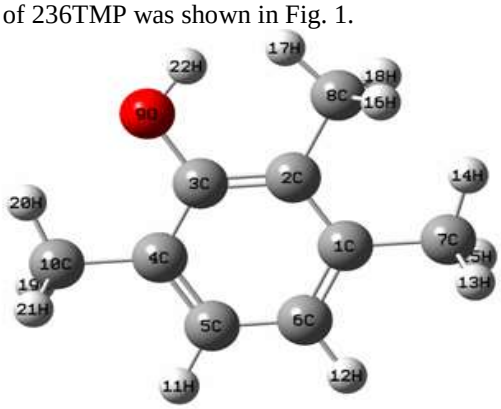

Fig. 1. The optimized molecular structure of 236TMP

Table 1. Total energies of 236TMP, calculated at DFT (B3LYP)/6-31G* and (B3LYP)/6-311+G level**

Method	Energies (Hartrees)
6-31G*	-425.2458714
6-311+G**	-425.4381749

Detailed description of vibrational modes can be given by means of normal coordinate analysis (NCA). For this purpose, the full set of 75 standard internal coordinates containing 15 redundancies were defined as given in Table 3. From these, a non-redundant set of local symmetry coordinates were constructed by suitable linear combinations of internal coordinates following the recommendations of Fogarasi et. al [10] are summarized in Table 4. The theoretically calculated DFT force fields were transformed in this later set of vibrational coordinates and used in all subsequent calculations.

Analysis of vibrational spectra

The 60 normal modes of 236TMP are distributed among the symmetry species as Γ_{3N-6}= 41 A' (in-plane) + 19 A″ (out-of-plane), and in agreement with C_s symmetry. All the vibrations were active both in Raman scattering and infrared absorption. In the Raman spectrum the in-plane vibrations (A') give rise to

polarized bands while the out-of-plane ones (A″) to depolarized band.

The detailed vibrational assignments of fundamental modes of 236TMP along with calculated IR, Raman intensities and normal mode descriptions (characterized by TED) were reported in Table 5. For visual comparison, the observed and simulated FT-IR and FT-Raman spectra of 236TMP are produced in a common frequency scales in Fig. 2 & Fig. 3.

Root mean square (RMS) values of frequencies were obtained in the study using the following expression,

$$RMS = \sqrt{\frac{1}{n-1}\sum_{i}^{n}\left(\upsilon_i^{calc} - \upsilon_i^{exp}\right)^2}$$

The RMS error of the observed and calculated frequencies (unscaled / B3LYP/6-311+G**) of 236TMP was found to be 127 cm^{-1}. This is quite obvious; since the frequencies calculated on the basis of quantum mechanical force fields usually differ appreciably from observed frequencies. This is partly due to the neglect of anharmonicity and partly due to the approximate nature of the quantum mechanical methods. In order to reduce the overall deviation between the unscaled and observed fundamental frequencies, scale factors were applied in the normal coordinate analysis and the subsequent least square fit refinement algorithm resulted into a very close agreement between the observed fundamentals and the scaled frequencies. Refinement of the scaling factors applied in this study achieved a weighted mean deviation of 6.4 cm^{-1} between the experimental and scaled frequencies of the title compound.

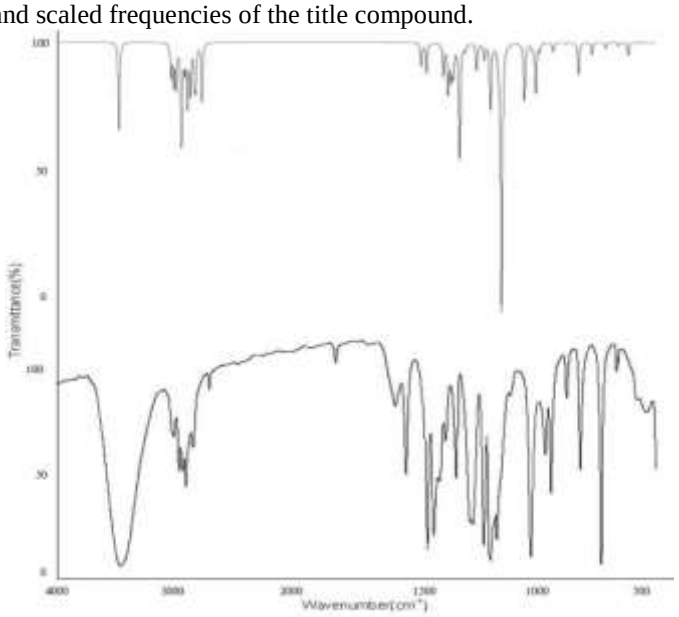

Fig. 2. FT-IR spectra of 236TMP
(a)Observed (b) Calculated with B3LYP/6-311+G**

C–H vibrations

The aromatic structure shows the presence of C–H stretching vibrations in the region 3000–3100 cm^{-1} which is the characteristic region for the ready identification of C–H stretching vibrations. This permits the ready identification of the structure. Further, in this region, the bands are not much affected due to the nature and position of the substitutions. The FT-IR bands at 3110, 3106 and 3103 cm^{-1} and FT-Raman bands at 3125, 3122 and 3120 cm^{-1} in 236TMP were assigned to C–H stretching modes. Overtone and combination bands due to the C–H out-of-plane deformation vibrations occur in the region 2000–1670 cm^{-1}. This absorption patterns observed at 1645, 1462 and 1322 cm^{-1} for FT-IR and 1676, 1552, 1465, 1296 and 1238 cm^{-1} for FT-Raman.

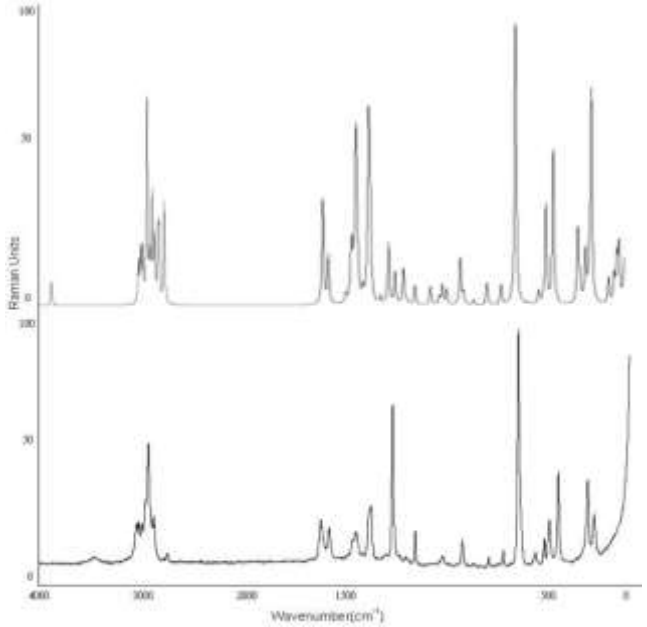

Fig. 3. FT-Raman spectra of 236TMP
(a) Observed (b) Calculated with B3LYP/6-311+G**

C-C vibrations

The ring C-C stretching vibrations, known as semicircular stretching usually occur in the region 1380-1280 and 1625-1430cm^{-1}. The C-C stretching vibrations of 236TMP are observed at 1645, 1642, 1641, 1462, 1461 and 1421 cm^{-1} in the FT-IR spectrum and 1676, 1675, 1670, 1552, 1550, 1549, 1465, 1430, 1429 and 1428 cm^{-1} in FT-Raman spectrum. In accordance with above literature data in our present study, the bands for C-C stretching vibrations are observed at 1379, 1370, 1368, 1330, 1326, 1322, 1256, 1250 and 1249 cm^{-1} in FT-IR spectrum and 1380, 1296, 1235 and 1233 cm^{-1} in FT-Raman spectrum. These observed frequencies show that, the substitutions in the ring to some extent about the ring mode of vibrations. The comparison of the theoretically computed values are in good agreement theoretical values obtained by B3LYP/6-311G** method.

C–O vibrations

If a compound contains a carbonyl group, the absorption caused by the C–O stretching is generally strongest. Considerations of these factors lead to assign the band observed at 1465, 1462, 1461, 1322, 1330, 1326, 1293, 1295, 1296, 1238, 1235 and 1233 cm^{-1} to C–O stretching vibrations for the title compound.

O-H vibrations

The O–H stretching vibrations are sensitive to hydrogen bonding. The O–H stretching vibration is normally observed at about 3500-3900 cm^{-1}. The O–H in-plane bending vibration is observed in the region 1440–1260 cm^{-1} [11]. In 236TMP, the bands appeared at 3840, 3841, 3845 and 3846 cm^{-1} are assigned to O–H stretching modes of vibration. The in-plane and out-of-plane bending vibrations of hydroxyl groups have been identified at 1380, 1379, 1370, 1330, 1326, 1322, 1293, 1295, 1296 and 1265 cm^{-1} for 236TMP.

Ring vibrations

Many ring modes are affected by the substitutions in the ring of 236TMP. In the present study the bands identified at 1110, 1109, 1108, 955, 953, 938, 936, 885, 883, 881, 744, 741, 736, 740, 666 and 662 cm^{-1} for 236TMP have been designated to ring in-plane and out-of-plane bending modes, respectively by careful consideration of their quantitative descriptions.

Table 2. Optimized geometrical parameters of 236TMP obtained by B3LYP/ 6–311+G density functional calculations**

Bond length	Value(Å)	Bond angle	Value(Å)	Dihedral angle	Value(Å)
C2-C1	1.38607	C3-C2-C1	119.99816	C4-C3-C2-C1	0.00000
C3-C2	1.38600	C4-C3-C2	119.99816	C5-C4-C3-C2	0.00000
C4-C3	1.38607	C5-C4-C3	120.00160	C6-C1-C2-C3	0.00000
C5-C4	1.38599	C6-C1-C2	120.00160	C7-C1-C6-C5	179.42864
C6-C1	1.38599	C7-C1-C6	119.99899	C8-C2-C1-C6	179.42861
C7-C1	1.54005	C8-C2-C1	119.99913	O9-C3-C2-C1	-179.42753
C8-C2	1.53998	O9-C3-C2	120.00070	C10-C4-C3-C2	-179.42865
O9-C3	1.40997	C10-C4-C3	119.99693	H11-C5-C4-C3	179.42803
C10-C4	1.54005	H11-C5-C4	119.99647	H12-C6-C1-C2	-179.42803
H11-C5	1.12197	H12-C6-C1	119.99647	H13-C7-C1-C6	-59.42785
H12-C6	1.12197	H13-C7-C1	109.49837	H14-C7-C1-C6	-179.49404
H13-C7	1.12200	H14-C7-C1	109.49495	H15-C7-C1-C6	60.64141
H14-C7	1.12203	H15-C7-C1	109.49819	H16-C8-C2-C1	-59.43016
H15-C7	1.12193	H16-C8-C2	109.49920	H17-C8-C2-C1	-179.49403
H16-C8	1.12197	H17-C8-C2	109.49750	H18-C8-C2-C1	60.64456
H17-C8	1.12197	H18-C8-C2	109.50235	H19-C10-C4-C3	120.00081
H18-C8	1.12192	H19-C10-C4	109.49837	H20-C10-C4-C3	-0.06537
H19-C10	1.12200	H20-C10-C4	109.49495	H21-C10-C4-C3	-119.92992
H20-C10	1.12203	H21-C10-C4	109.49819	H22-O9-C3-C2	0.00387
H21-C10	1.12193	H22-O9-C3	109.49778		
H22-O9	0.99204				

*for numbering of atom refer Fig.1

Table 3. Definition of internal coordinates of 236TMP

No(i)	symbol	Type	Definition
Stretching 1-6	r_i	C-C	C2-C3,C3-C4,C4-C5,C5-C6,C3-C10, C5-C11
7	S_i	C-O	C3-O9
8-9	p_i	C-H	C5-H11,C6-H12
10-12	s_i	C-C(m)	C1-C7,C2-C8,C4-C10
13	N_i	O-H	O9-H22
14-16	P_i	C-H(m)	C7-H13,C7-H14,C7-H15
17-19	Φ_i	C-H(m)	C8-H16,C8-H17,C8-H18
20-22	ψ_i	C-H(m)	C10-H19+C10-H20+C10-H21
Bending 23-28	α_i	C-C-C	C1-C2-C3,C2-C3-C4,C3-C4-C5, C4-C5-C6,C5-C6-C1,C6-C1-C2
29-32	θ_i	C-C-H	C4-C5-H11, C6-C5-H11, C5-C6-H12, C1-C6-H12.
33-34	β_i	C-C-O	C2-C3-O9, C4-C3-O9
35	n_i	C-O-H	C3-O9-H22
36-41	ε_i	C-C-C	C6-C1-C7, C2-C1-C7, C1-C2-C8, C3-C2-C8, C3-C4-C10, C5-C4-C10
42-44	γ_i	H-C-H	H13-C7-H14,H14-C7-H15,H15-C7-H13
45-47	μ_i	C-C-H	C1-C7-H13,C1-C7-H14, C1-C7-H15
48-50	ν_i	H-C-H	H16-C8-H17,H17-C8-H18, H18-C8-H16
51-53	φ_i	C-C-H	C2-C8-H16,C2-C8-H17, C2-C8-H18
54-56	ι_i	H-C-H	H19-C10-H20, H20-C10-H21, H21-C10-H19
57-59	ϖ_i	C-C-H	C4-C10-H19,C4-C10-H20,C4-C10-H21
Out-of-plane 60-61	ω_i	C-H	H11-C5-C4-C6, H12-C6-C5-C1
62	ξ_i	C-O	O9-C3-C4-C2
63-65	Ω_i	C-C	C7-C1-C6-C2, C8-C2-C3-C1, C10-C4-C5-C3
Torsion 66-71	τ_i	C-C	C1-C2-C3-C4,C2-C3-C4-C5, C3-C4-C5-C6,C4-C5-C6-C1, C5-C6-C1-C2,C6-C1-C2,C3
72	τ_i	C-C-H	C6-C1-C7-(H13,H14,H15)

73	τ_i	C-C-H	C1-C2-C8-(H16,H17,H18)
74	τ_i	C-C-H	C3-C4-C10-(H19,H20,H21)
75	τ_i	O-H	C2(C4)-C3-O9-H22

*for numbering of atom refer Fig.1

Table 4. Definition of local symmetry coordinates and the value corresponding scale factors used to correct the force fields for 236TMP

No.(i)	Symbol[a]	Definition[b]	Scale factors used in calculation
1-6	C-C	r1,r2,r3,r4,r5,r6	0.914
7	C-O	S7	0.914
8-9	C-H	P8, p9	0.992
10-12	C-C(m)	S10,s11,s12	0.992
13	O-H	N13	0.919
14	mss1	(P14+P15+P16)/ √3	0.995
15	mips1	(2P15-P14-P16)/ √6	0.992
16	mops1	(P15-P16)/ √2	0.919
17	mss2	(Φ17+Φ18+Φ19)/ √3	0.995
18	mips2	(2Φ18-Φ17-Φ19)/ √6	0.992
19	mops2	(Φ18-Φ19)/ √2	0.919
20	mss3	(ψ20+ψ21+ψ22)/ √3	0.995
21	mips3	(2ψ21-ψ20-ψ22)/ √6	0.992
22	mops3	(ψ21-ψ22)/ √2	0.919
23	C-C-C	(α23-α24+α25-α26+α27-α28)/ √6	0.992
24	C-C-C	(2α23-α24-α25+2α26-α27-α28)/ √12	0.992
25	C-C-C	(α24-α25+α27-α28)/2	0.992
26-27	C-C-H	(θ29-θ30)/√2,(θ31-θ32)/√2	0.916
28	C-C-O	(β33-β34)/√2	0.923
29	C-O-H	n35	0.923
30-32	C-C-C	(ε36-ε37)/√2, (ε38-ε39)/√2, (ε40-ε41)/√2	0.923
33	msb1	(γ42+γ43+γ44-μ45-μ46-μ47)/ √6	0.990
34	mipb1	(2γ44-γ42-γ43)/ √6	0.990
35	mopb1	(γ42-γ44)/ √2	0.990
36	mipr1	(2μ46-μ45-μ47)/ √6	0.990
37	mopr1	(μ45-μ47)/ √2	0.990
38	msb2	(ν48+ν49+ν50-φ51-φ52-φ53)/ √6	0.990
39	mipb2	(2ν50-ν48-ν49)/ √6	0.990
40	mopb2	(ν48-ν50)/ √2	0.990
41	mipr2	(2φ52-φ51-φ53)/ √6	0.990
42	mopr2	(φ51-φ53)/ √2	0.990
43	msb3	(ι54+ι55+ι56-ϖ57-ϖ58-ϖ59)/ √6	0.990
44	mipb3	(2ι56-ι54-ι55)/ √6	0.990
45	mopb3	(ι54-ι56)/ √2	0.990
46	mipr3	(2ϖ58-ϖ57-ϖ59)/ √6	0.990
47	mopr3	(ϖ57-ϖ59)/ √2	0.990
48-49	C-H	ω60,ω61	0.994
50	C-O	ξ62	0.994
51-53	C-C	Ω63, Ω64, Ω65	0.962
54	tring	(τ66-τ67+τ68-τ69+τ70-τ71)/√6	0.994
55	tring	(τ66-τ68+τ69-τ71)/2	0.994
56	tring	(-τ66+2τ67-τ68-τ69+2τ70-τ71)/√12	0.994
57	C-C-H	τ72/3	0.979
58	C-C-H	τ73/3	0.979
59	C-C-H	τ74/3	0.979
60	O-H	τ75/2	0.979

[a] These symbols are used for description of the normal modes by TED in Table 5.
[b] The internal coordinates used here are defined in Table 3.

Table 5. Detailed assignments of fundamental vibrations of 236TMP by normal mode analysis based on SQM force field calculation

S. No.	Symmetry species C_s	Observed frequency (cm^{-1})		Calculated frequency (cm^{-1}) with B3LYP/6-311+G** force field				TED (%) among type of internal coordinates[c]
		Infrared	Raman	Unscaled	Scaled	IR[a] A_i	Raman[b] I_i	
1	A'	3845	3846	3841	3840	44.916	71.387	OH(100)
2	A'			3189	3188	15.791	65.164	mips2(84),mops2(9),mss2(6)
3	A'	3180	3176	3175	3172	19.919	82.894	mips3(97)
4	A'		3150	3158	3156	22.005	80.140	mips1(94)
5	A'	3125		3126	3125	36.179	265.265	mss3(86),CH(11)
6	A'		3125	3122	3120	24.939	81.725	CH(88),mss3(11)
7	A'	3110		3106	3103	11.222	56.467	CH(98)
8	A'			3087	3086	30.738	154.100	mss1(87),mops1(7)
9	A'		3070	3069	3068	24.404	90.837	mss2(41),mops2(41),mips2(17)
10	A'	3048		3045	3043	17.198	82.685	mops3(98)
11	A'	3031	3037	3036	3035	20.540	93.199	mops1(89),mss1(9)
12	A'			2997	2996	29.974	138.777	mss2(51),mops2(49)
13	A'		1676	1675	1670	11.934	37.984	CC(65),bring(10),bCH(9)
14	A'	1645		1642	1641	15.405	16.709	CC(64),bring(11),bCH(6)
15	A'		1552	1550	1549	16.657	2.732	CC(34),bCH(24),bmipb2(14),CCm(8)
16	A'	1530		1525	1523	24.169	9.372	bmopb1(58),bmipb1(21)
17	A'		1520	1519	1518	0.088	11.836	bmopb2(45),bmipb2(32),bmipb1(17),bmopb1(6)
18	A'			1510	1508	15.366	6.707	bmipb3(39),bmipb2(24),bmopb1(11),bmipb1(6),bCH(5),CC(5)
19	A'	1495		1499	1498	9.537	27.753	bmipb1(38),bmopb2(30),bmipb2(21),bmopb1(9)
20	A'		1498	1497	1496	3.487	17.312	bmopb1(43),bmipb2(26),bmipb1(19)
21	A'	1494		1492	1491	4.994	20.273	bmopb3(55),bmipb3(43)
22	A'	1462	1465	1462	1461	59.296	3.179	CC(31),bmopb1(15),bmipb3(12),CO(12),bCH(8),bmipb1(5)
23	A'			1433	1432	2.655	41.328	bmsb1(59),bmsb2(23),CCm(6)
24	A'		1430	1429	1428	0.803	11.225	bmsb3(76),CCm(9),bmsb1(8)
25	A'	1421		1425	1422	0.828	24.290	bmsb2(62),bmsb1(20),bmsb3(8),CCm(7)
26	A"	1379	1380	1370	1368	13.811	1.745	gCC(70),bCOH(12)
27	A'	1322		1330	1326	8.040	14.732	CC(35),bCH(18),CO(17),CCm(10),bCOH(7)
28	A'		1296	1295	1293	33.944	7.248	bCH(32),CC(15),CCm(13),bring(9),CO(8),bCOH(5)
29	A'	1256		1250	1249	8.256	7.790	CCm(34),bring(32),CC(13),bCOH(8)
30	A'		1238	1235	1233	137.583	0.988	bCOH(35),CC(23),CCm(14),CO(11),bCH(7),bring(6)
31	A"	1194		1191	1189	0.296	3.858	gCC(52), bCH(31),CCm(11)
32	A'		1110	1109	1108	29.511	3.355	CCm(22),bmopr2(19),CO(11),bring(8),bmopr1(8),bmipr2(6)
33	A"	1079		1070	1069	2.389	0.098	gCC(31), bmipr1(9),bmipb1(9),bmopr1(8),bmipr3(8),bmipr2(5)
34	A"			1063	1062	0.669	1.205	tring(34),bmopb3(13),bmipb3(11),bmopr3(9),bmipr1(9), bmipr3(7)
35	A'	1045	1048	1048	1047	12.044	1.579	bmipr2(20),bmopr2(19),bmopr3(15),bmopb2(9),bmipb2(6),bmipr1(6)
36	A'			1049	1046	13.909	1.620	bmipr2(30),bmopr3(17),CC(8),bmipb2(7),bmopb2(7),bmipr3(6)
37	A'	1028	1026	1025	1024	4.165	2.414	bmopr1(38),bmopr2(14),CC(13),bmopb1(6),bmipr1(6)
38	A"			955	953	4.803	6.699	gCC(23),CCm(22),bmopr3(13),bmopr1(10),bring(9)
39	A"	936	938	938	936	0.198	1.613	gCH(87),tring(9)
40	A'	881		885	883	0.705	0.649	CCm(22),bring(20),CC(20),bmopr2(14),CO(10)
41	A"		816	815	813	16.416	2.483	gCH(90)
42	A"	736		744	741	1.493	0.280	tring(57),gCO(19),gCC(17)
43	A'			742	740	4.733	1.654	bring(46),CCm(39),CC(5)
44	A"	666	662	668	665	3.338	23.712	CC(44),CCm(29),CO(11),bring(8)
45	A"	605		599	598	1.905	0.129	tring(43),gCC(27),gCO(24)
46	A'		537	546	544	6.917	0.829	bCCO(26),bCC1(22),bCC3(15),bCC2(13),CC(7)
47	A"	522	512	522	521	0.005	0.080	tring(49),gCC(39)
48	A'	502		508	506	0.141	5.587	bring(62),CCm(12),bCCO(8),CC(7),CO(5)
49	A'		468	469	468	0.582	7.766	bring(64),CCm(17),CC(9)
50	A"			340	339	44.346	2.215	tOH(40),gCC(32),tring(9)
51	A'		325	339	338	1.328	0.076	bCC2(60),bCCO(21),bring(8)
52	A'			330	327	1.502	0.661	bCC1(58),bCCO(21),bring(8),CC(7)
53	A"		296	300	299	42.337	1.302	gCC(38),tOH(27),tring(15),bmopb2(5)
54	A'			285	282	1.938	0.451	bCC3(64),bCC2(11),CC(6)
55	A"		276	275	270	8.321	4.633	gCC(51),tOH(16),gCO(15),tring(10)
56	A"			185	179	0.026	0.279	tCH31(87)
57	A"		150	155	150	0.013	0.211	tring(45),gCC(13),tCH33(12),tCH32(10)
58	A"			139	136	2.258	0.292	tring(46),gCC(19),tCH33(12),gCH(8)
59	A"		128	127	125	0.000	0.317	tCH33(65),tring(13),gCC(6),bmopb3(6)
60	A"			93	91	1.449	0.524	tCH32(56),tring(20),tOH(7),bmopb2(5)

Abbreviations used: b, bending; g, wagging; t, torsion; s, strong; vs, very strong; w, weak; vw, very weak;

[a] Relative absorption intensities normalized with highest peak absorption

[b] Relative Raman intensities calculated by Eq.1 and normalized to 100.

[c] For the notations used see Table 4.

Table 6. The dipole moment (μ) and first-order hyperpolarizibility (β) of 236TMP derived from DFT calculations

β_{xxx}	-241.33
β_{xxy}	-30673
β_{xyy}	-568.24
β_{yyy}	4281
β_{zxx}	151.17
β_{xyz}	-1841.3
β_{zyy}	-30.213
β_{xzz}	-404.95
β_{yzz}	6660.3
β_{zzz}	-64.498
β_{total}	93.99
μ_x	0.51066459
μ_y	2.531
μ_z	0.05208355
μ	0.75018228

Dipole moment (μ) in Debye, hyperpolarizibility $\beta(-2\omega;\omega,\omega)$ 10^{-30}esu.

Table 7. Computed absorption wavelength (λ_{ng}) , energy (E_{ng}), oscillator strength (f_n) and its major contribution

n	λ_{ng}	E_{ng}	f_n	Major contribution
1	201.6	6.15	0.0360	H-0->L+0(+57%), H-1->L+1(29%)
2	195.6	6.34	0.0142	H-1->L+0(+44%), H-0->L+1(+39%)
3	152.5	8.13	0.9590	H-0->L+1(+38%), H-1->L+0(35%)

(Assignment; H=HOMO,L=LUMO,L+1=LUMO+1,etc.)

A small change in frequencies observed for these modes are mainly due to the presence of methyl group in 236TMP and from different extents of mixing between ring and constituent group vibrations.

Methyl group vibrations

The title compound 236TMP, the assignments of CH_3 group frequencies, one can expect that nine fundamentals can be associated to each CH_3 group, namely the symmetrical (m ips) and asymmetrical (m ops), inplane stretching modes (i.e. in-plane hydrogen stretching mode); the symmetrical (m ss), and asymmetrical (m ips), deformation modes; the in-plane rocking (m ipr) and out-of-plane rocking (m opr) modes. In addition to that, the asymmetric stretching (m ops) and asymmetric deformation (m opb) modes of the CH_3 group are expected to be depolarised for A'' symmetry species. The infrared band found at 3180, 3125, 3126, 3048, 3031 cm^{-1} and 3176, 3150, 3125, 3070, 3037 cm^{-1} represent symmetric and asymmetric CH_3 stretching vibrations of the methyl group in 236TMP. The fundamental vibrations arising from symmetric, asymmetric in-plane and out-of-plane deformations, rocking and twisting modes of CH_3 group of 236TMP are observed in their respective characteristic regions and they are tabulated.

Hyperpolarizability calculations

The first-order hyperpolarizibility (β_{ijk}) of the novel molecular system of 236TMP is calculated using 3-21 G (d,p) basis set based on finite field approach. Hyperpolarizibility is a third rank tensor that can be described by a 3 x 3 x 3 matrix. It strongly depends on the method and basis set used. The 27 components of 3D matrix can be reduced to 10 components due to Kleinman [12] symmetry. The calculated first-order hyperpolarizability (β_{total}) of 236TMP is 93.99×10^{-30} esu, which is nearly 482 times greater than that of urea (0.1947×10^{-30} esu). The calculated dipole moment (μ) and first-order hyperpolarizibility (β) are shown in Table 6.

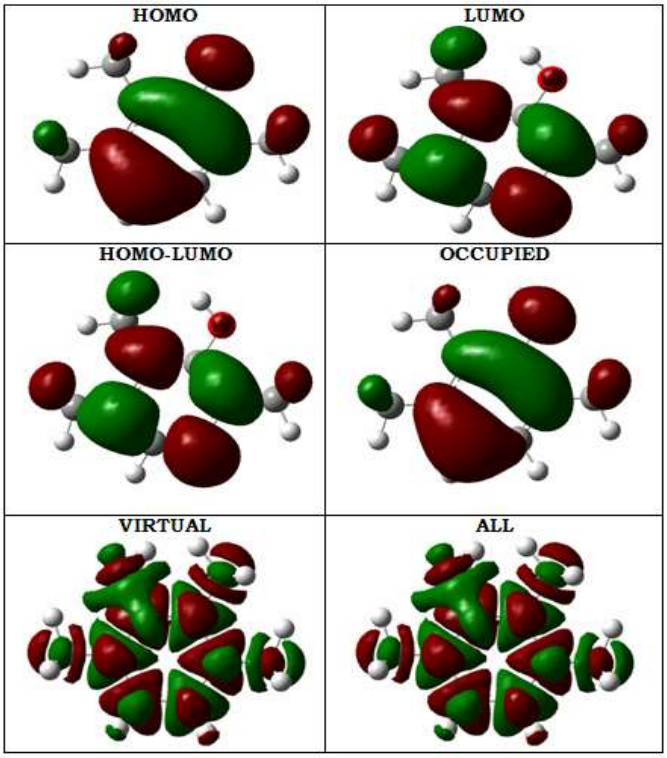

Fig. 4. Representation of the orbital involved in the electronic transition for (a) HOMO (b) LUMO (c) HOMO, LUMO (d) Occupied (e) Virtual (f) All

The theoretical calculation seems to be more helpful in determination of particular components of β tensor than in establishing the real values of β. Domination of particular components indicates on a substantial delocalization of charges in those directions. It is noticed that in β_{yzz} (which is the principal dipole moment axis and it is parallel to the charge transfer axis) direction, the biggest values of hyperpolarizability

are noticed and subsequently delocalization of electron cloud is more in that direction. The higher dipole moment values are associated, in general, with even larger projection of β_{total} quantities. The electric dipoles may enhance, oppose or at least bring the dipoles out of the required net alignment necessary for NLO properties such as β_{total} values. The connection between the electric dipole moments of an organic molecule having donor–acceptor substituent and first hyperpolarizability is widely recognized in the literature [13]. The maximum β was due to the behavior of non-zero μ value. One of the conclusions obtained from this work is that non-zero μ value may enable the finding of a non-zero β value. Of course Hartee–Fock calculations depend on the mathematical method and basis set used for a polyatomic molecule.

Fig. 4. shows the highest occupied molecule orbital (HOMO) and lowest unoccupied molecule orbital (LUMO) of 236TMP. There is an inverse relationship between hyperpolarizability and HOMO–LUMO.

HOMO energy = -0.206 a.u

LUMO energy = 0.009 a.u

HOMO–LUMO energy gap = 0.125 a.u

Electronic excitation mechanism

The static polarizability value[14-15] is proportional to the optical intensity and inversely proportional to the cube of transition energy. With this concept, larger oscillator strength (f_n) and $\Delta\mu_{gn}$ with lower transition energy (E_{gn}) is favourable to obtain large first static polarizability values. Electronic excitation energies, oscillator strength and nature of the respective excited states were calculated by the closed-shell singlet calculation method and are summarized in Table 7. Representation of the orbital involved in the electronic transition was shown in Fig. 5.

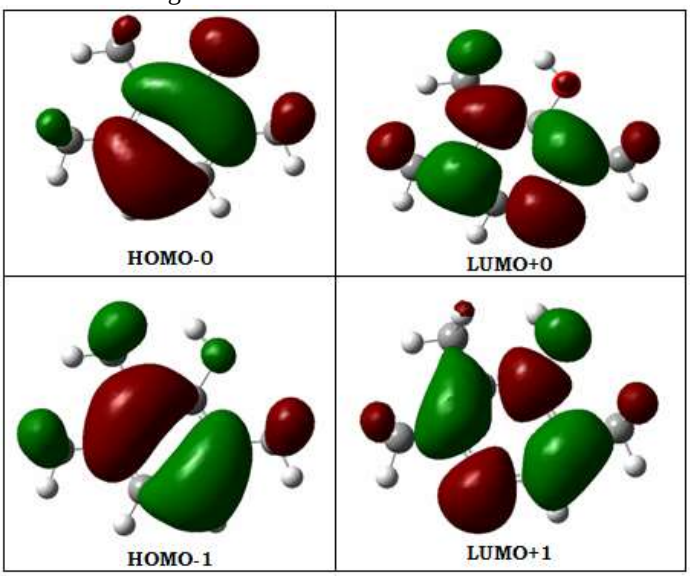

Fig. 5. Representation of the orbital involved in the electronic transition for (a) HOMO-0 (b) LUMO+0 (c) HOMO-1 (d) LUMO+1

Conclusions

IR and Raman Spectra were obtained for 236TMP, in which all of the expected 60 normal modes of vibration were assigned. The optimized molecular geometry, force constants and vibrational frequencies were calculated using DFT techniques in the B3LYP approximation. Taking the observed frequencies as a basis corresponding to the fundamental vibrations, it was possible to proceed to a scaling of the theoretical force field. The resulting SQM force field served to calculate the potential energy distribution, which revealed the physical nature of the molecular vibrations, and the force constants in internal coordinates, which were similar to the values obtained before for related chemical species. The first-order hyperpolarizibility (β_{ijk}) of the novel molecular system of 236TMP is calculated using 6-311+G** basis set based on finite field approach. The first-order hyperpolarizability (β_{total}) of 236TMP was calculated and found to be 93.99×10^{-30} esu, which is nearly 482 times greater than that of urea (0.1947×10^{-30} esu). Hence these materials have been motivated by their wide range of potential applications such as second harmonic generation (SHG), electro-optic modulation, sum and difference frequency doubling of lasers, etc. Such materials have large nonlinear optical coefficients, suitable transparency and excellent comprehensive properties. Electronic excitation energies, oscillator strength and nature of the respective excited states were calculated by the closed-shell singlet calculation method.

Reference

1. M. J. Frisch, G. W. Trucks, H. B. Schlegel, G. E. Scuseria, M. A. Robb, J. R. Cheeseman, J. A. Montgomery, Jr., T. Vreven, K. N. Kudin, J. C. Burant, J. M. Millam, S. S. Iyengar, J. Tomasi, V. Barone, B. Mennucci, M. Cossi, G. Scalmani, N. Rega, G. A. Petersson, H. Nakatsuji, M. Hada, M. Ehara, K. Toyota, R. Fukuda, J. Hasegawa, M. Ishida, T. Nakajima, Y. Honda, O. Kitao, H. Nakai, M. Klene, X. Li, J. E. Knox, H. P. Hratchian, J. B. Cross, C. Adamo, J. Jaramillo, R. Gomperts, R. E. Stratmann, O. Yazyev, A. J. Austin, R. Cammi, C. Pomelli, J. W. Ochterski, P. Y. Ayala, K. Morokuma, G. A. Voth, P. Salvador, J. J. Dannenberg, V. G. Zakrzewski, S. Dapprich, A. D. Daniels, M. C. Strain, O. Farkas, D. K. Malick, A. D. Rabuck, K. Raghavachari, J. B. Foresman, J. V. Ortiz, Q. Cui, A. G. Baboul, S. Clifford, J. Cioslowski, B. B. Stefanov, G. Liu, A. Liashenko, P. Piskorz, I. Komaromi, R. L. Martin, D. J. Fox, T. Keith, M. A. Al-Laham, C. Y. Peng, A. Nanayakkara, M. Challacombe, P. M. W. Gill, B. Johnson, W. Chen, M. W. Wong, C. Gonzalez, and J. A. Pople, Gaussian, Inc., Pittsburgh PA, 2003.
2. A.D. Becke, J. Chem. Phys., 98 (1993) 5648.
3. P. Pulay, G. Fogarasi, G.Pongor, J. E. Boggs, A. Vargha, J. Am. Chem. Soc., 105 (1983) 7037.
4. T. Sundius, J. Mol. Struct., 218 (1990) 321.
5. F.A. Cotton, Chemical Applications of Group Theory, Wiley Interscience, New York, 1971.
6. A. Frisch, A.B. Nielson, A.J. Holder, GAUSSVIEW Users Manual, Gaussian Inc., Pittsburgh, PA, 2000.
7. P.L. Polavarapu, J. Phys. Chem. 94, 8106 (1990).
8. G. Keresztury, S. Holly, J. Varga, G. Besenyei, A.V. Wang, J.R. Durig, Spectrochim. Acta 49A,2007 (1993).
9. G. Keresztury, in: J.M. Chalmers and P.R. Griffiths(Eds), Handbook of Vibrational Spectroscopy vol.1, John Wiley & Sons Ltd. p. 71, (2002).
10. P. Pulay, G. Fogarasi, F. Pong, J.E. Boggs, J. Am. Chem. Soc.,101 (1979) 2550.
11. D.N. Sathyanarayan, Vibrational Spectroscopy, Theory and Applications, second ed., New Age International (P) Limited Publishers, New Delhi, 2004.
12. D.A. Kleinman, Phys. Rev. 1962;126,1977.
13. P.N. Prasad, D.J. Williams, Introduction to Nonlinear Optical Effects in Molecules and Polymers, Wiley, New York, 1991.
14. K. Wu, C. Liu, C. Mang, Opt. Mater. 29 (2007) 1129–1137.
15. S. Iran, W.M.F. Fabian, Dyes Pigments 70 (2006) 91–96.